# Characteristics of tropical cyclones in high-resolution models of the present climate

Daniel A. Shaevitz[1]

Suzana J. Camargo[2*], Adam H. Sobel[1,2,3], Jeffrey A. Jonas[4,5], Daeyhun Kim[2], Arun Kumar[6], Timothy E. LaRow[7], Young-Kwon Lim[8], Hiroyuki Murakami[9], Malcolm J. Roberts[10], Enrico Scoccimarro[11], Hui Wang[6], Michael F. Wehner[12], Ming Zhao[13]

*1 Department of Applied Physics and Applied Mathematics, Columbia University, New York, NY*

*2 Lamont-Doherty Earth Observatory, Columbia University, Palisades, NY*

*3 Department of Earth and Environmental Sciences, Columbia University, New York, NY*

*4 Center for Climate System Research, Columbia University, New York, NY*

*5 NASA Goddard Institute for Space Studies, New York, NY*

*6 NOAA/NWS/NCEP Climate Prediction Center, College Park, MD*

*7 Center for Ocean Atmospheric Prediction Studies, Florida State University, Tallahasee, FL*

*8 NASA Goddard Space Flight Center, Greenbelt, MD*

*9 International Pacific Research Center, University of Hawaii at Manoa, Honolulu, HI*

*10 Met Office, Hadley Center, Devon, United Kingdom*

*11 Ilstituto Nazionale di Geofisica and Vulcanologia, Bologna, Italy*
*and Centro Euro-Mediterraneo per i Cambiamenti Climatici, Lecce, Italy*

*12 Lawrence Berkeley National Laboratory, Berkeley, CA, and University of California, Berkeley, Berkeley, CA*

*13 NOAA Geophysical Fluid Dynamics Laboratory, Princeton, NJ*

[*] *Corresponding author address:* Suzana J. Camargo Lamont-Doherty Earth Observatory Columbia University PO Box 1000, Palisades, NY 10960.

E-mail: suzana@ldeo.columbia.edu

ABSTRACT

The global characteristics of tropical cyclones (TCs) simulated by several climate models are analyzed and compared with observations. The global climate models were forced by the same sea surface temperature (SST) in two types of experiments, using a climatological SST and interannually varying SST. TC tracks and intensities are derived from each model's output fields by the group who ran that model, using their own preferred tracking scheme; the study considers the combination of model and tracking scheme as a single modeling system, and compares the properties derived from the different systems. Overall, the observed geographic distribution of global TC frequency was reasonably well reproduced. As expected, with the exception of one model, intensities of the simulated TC were lower than in observations, to a degree that varies considerably across models.

## 1. Introduction

The impact of tropical cyclones (TCs) on society makes it important to understand how their characteristics might change in the future. Global climate models, also known as General Circulation Models (GCMs), are important tools for studying this problem. In a GCM, one has the ability to simulate the climate organically; if the model has sufficient resolution and physics to provide a plausible simulation of TCs as well, then one can use the model to examine how climate controls the statistical properties of TCs. One can explore, in particular, the behavior of TCs under different climate scenarios.

Many studies (e.g. Manabe et al. 1970; Bengtsson et al. 1982; Vitart et al. 1997; Camargo et al. 2005) have shown that GCMs, even at relatively low resolution, are capable of generating storms that have similar characteristics as observed TCs. More recently, studies that have used higher resolution atmospheric GCMs forced with prescribed sea surface temperatures (SSTs) (e.g. Bengtsson et al. 2007a; LaRow et al. 2008; Zhao et al. 2009) have demonstrated these high-resolution models' remarkable ability to simulate realistic distributions of TCs.

In order to use GCMs for projections of possible future changes in TC activity, it is necessary to assess their ability to reproduce the characteristics of observed TCs in the present climate. These characteristics include the climatological spatial, temporal, and intensity distributions as well as the interannual variability of TCs. This work is an intercomparison of the ability of 9 high-resolution GCMs to simulate TCs. The models have resolutions that vary from 28 to 130 km, with different parameterizations. Two of the models have done simulations at multiple resolutions, while a single resolution is available for our analysis of the other models.

The simulations analyzed were performed for the U.S. CLIVAR Hurricane Working Group. The objective of this working group was to have a better understanding of the differences among high-resolution models in simulating TC activity, in the present climate as well as in future climate scenarios. In order to do that, a set of common experiments with the same forcings and fixed SST was performed by all modeling groups. Here we analyze the characteristics of TC activity in the simulations of climate produced by the working group over SST distributions derived from observations taken in the late 20th century (1981-2005 for the climatology simulations and 1981-2009 for the interannual simulations).

Observed TC tracks and intensities are derived from atmospheric measurements — in situ and remote — by human forecasters. With climate models, it is necessary to apply objective tracking schemes to the model output fields to obtain the tracks and intensities. The criteria applied to the models can be different than those applied to observations; a model storm is not necessarily required to meet the same thresholds for intensity as an observed one would be in order to be classified as a TC. It has been found that when allowance is made for the fact that model TCs are weaker and larger than those observed, the resulting spatio-temporal distributions of TC tracks resemble those observed enough to be useful — for example, in seasonal forecasting — even in quite low-resolution models (Camargo and Barnston 2009; Camargo et al. 2010).

In the present study, we examine the TCs derived from each model's output by the group who ran that particular model, using their own preferred tracking scheme. We consider the combination of model and tracking scheme to be a "modeling system" and compare the outputs from each system. In the interests of brevity, we will refer to these modeling systems below simply as "models", taking the tracking scheme as implicit, though our expectations about the sensitivities of the results to tracking schemes are discussed in several points.

This approach implicitly makes allowances for the different resolutions and physics of each model, resulting in different TC intensities. It is consistent with the way each model has been used in previous single-model studies. Using each group's own tracks also allows each model to be seen in the best light, to the extent that tracking schemes have tunable parameters whose adjustment can allow some gross aspects of the statistics to be brought closer to those observed.

It is also of interest to compare the different models using the same tracking scheme, so that the differences in results are purely attributable to the differences in the models themselves. This work is underway and will be reported in due time.

This paper is organized as follows. The data, models, and experiments are discussed in section 2. Results from the climatological and historical forced models are described in section 3. Finally, conclusions are given in section 4.

# 2. Models and data

The data used for this study consists of TC tracks from nine GCMs. The models were forced with two different SST boundary conditions, climatologically averaged SSTs and monthly interannually varying SSTs. The SSTs were obtained from the Hadley Centre Sea Ice and Sea Surface Temperature (HadISST) data set (Rayner et al. 2003). Each group used the output of their simulations to detect and track the model TCs, using their own tracking algorithm. Tracks for these TCs were generated and their characteristics were analyzed here. The sensitivity of the models to the different tracking schemes is currently being analyzed by members of the working group.

Output from nine GCMs were analyzed in this study, as summarized in table 1, namely: Community Atmospheric Model version 5.1, or CAM5.1 (Wehner et al. 2013); European Center for Medium range Weather Forecasting - Hamburg, or ECHAM5 (Roeckner 2003; Scoccimarro et al. 2011); Florida State University, or FSU (LaRow et al. 2008); NASA Goddard Earth Observing System Model version 5, or GEOS-5 (Rienecker et al. 2008); National Center for Environmental Prediction Global Forecasting System, or GFS (Saha et al. 2013); NASA Goddard Institute for Space Studies, or GISS (Schmidt 2013); Met Office Hadley Centre Model version 3, or HadGEM3 (Walters et al. 2011); Geophysical Fluid Dynamics Laboratory High Resolution Atmosphere Model, or HiRAM (Zhao et al. 2009); and Meteorological Research Institute, or MRI (Mizuta et al. 2012; Murakami et al. 2012). The model resolutions vary from 28 to 111 km. The models have different tracking schemes, most of them with very similar characteristics, based on the original tracking schemes in

Bengtsson et al. (1982) and Vitart et al. (2007). These tracking schemes look for vortices with a minimum of sea level pressure, a maximum of low-level vorticity and a warm core (Camargo and Zebiak 2002; Walsh 1997; Vitart et al. 2003; Zhao et al. 2009; Murakami et al. 2012). The main difference among the schemes is how they define the warm core and the thresholds used to define the model TC. An exception is the HadGEM3, which uses a tracking scheme originally developed for extra-tropical (cold core) cyclones (Hodges 1995) and modified to track warm core vortices (Bengtsson et al. 2007a; Strachan et al. 2013).

We compare the model TCs characteristics with the observed TC data. For the North Atlantic and eastern and central North Pacific the best-track datasets from the National Hurricane Center is used (Landsea and Franklin 2013; NHC 2013). In the case of the western North Pacific, North Indian Ocean and southern hemisphere, the TC data is from the best-track datasets from the Joint Typhoon Warning Center (Chu et al. 2002; JTWC 2013).

# 3. Results

## *a. Climatology*

### 1) TC Frequency

There are on average approximately 80 TCs observed every year across the globe (Emanuel 2003). Figure 1 shows the distribution of the number of TCs per year for all models along with the observations. There are large differences in the number of TCs between the different models. Different models run at approximately the same resolution do not have similar mean numbers of TCs (e.g. the LR CAM5.1, FSU, GFS, and GISS models all have resolutions of roughly 100 km, but the mean number of TCs per year varies from about 10 to over 100.)

At the same time, the absolute number of TCs in each model is somewhat dependent on the tracking scheme applied; higher thresholds result in fewer TCs. Application of strictly uniform tracking schemes, with no allowance for the different intensities in different models (whether due to resolution or other factors) would almost certainly produce even larger differences in the total numbers of TCs from model to model. By using each group's own tracking scheme, we allow some compensation for the different TC intensities, in order to allow more productive comparison between other aspects of the results, such as the spatial and seasonal distributions of TC genesis and tracks, in the way that they would be shown in single-model studies by the individual groups.

The three resolutions of the HadGEM3 model show an increase in the number of TCs with increasing resolution, though it does not increase linearly. The tracking algorithm for all resolutions of the HadGEM3 model use the same threshold for the 850-hPa relative vorticity after being filtered to a standard spectral resolution of T42 as described in Strachan et al. (2013). Thus, the increase in the number of TCs with increasing resolution is not an artifact of the tracking scheme.

Figure 2 shows the mean number of TCs formed per year in each ocean basin. The total number of TCs formed in each basin per year is shown at the top of the figure and the percentage of all TCs that formed in each basin is shown at the bottom. Due to the large differences in the total numbers of global TCs reported by each model, it is more illustrative to compare the percentages of the TCs that form in each basin, rather than the total number of TCs, to the observations.

There are clear differences between the models in the distribution of TCs across, particularly in the North Atlantic and Pacific. Several of the models (ECHAM5, GISS, and all resolutions of the HadGEM) have percentages much lower than that observed in the North Atlantic. Three of the models (ECHAM5, FSU, and GISS) have a significantly lower percentage than that observed in the Eastern North Pacific, while the CAM5.1 (at both resolutions) and the GEOS-5 model have a much higher percentage than observed in the Eastern North Pacific. In the Western North Pacific, the CAM5.1 models have smaller percentages than observed, and the ECHAM5 and GISS models have larger percentages than observed.

This is consistent with previous studies that have found that low-resolution models tend to have a large percentage of TCs in the Western North Pacific and very few TCs in the North Atlantic (Camargo et al. 2005; Camargo 2013).

One interesting observation is that there is a larger difference in TC distributions among the different models, than among different resolutions of the same model. The TC distributions of the different resolutions of the CAM5.1 and HadGEM3 models are very similar. This suggests that the global and regional distributions of TCs is mainly determined by the characteristics of the models (e.g. parameterizations, convection scheme), with model resolution not being as important. While the tracking schemes are also different, our expectation is that the usage of different tracking schemes reduces the apparent differences between models, particularly in overall TC frequency. As will be seen below, the intensities of the simulated TCs are quite different in different models, and the different thresholds in the tracking schemes adjust for this to a large degree. If the same tracking scheme (including the specific thresholds) used to detect TCs in HiRAM were applied to the GISS model, for example, very few TCs would be detected.

In order to study the geographic patterns of TC occurrence, we will use track density, defined as the total number of TCs that pass through a 5° x 5° box per year. Figure 3 shows the track density distributions for all models and observations. The distribution of observed track density shows a region of very high density off the western coast of Central America and the eastern coast of Asia, along with regions of high density in the North Atlantic, South Indian, and off the eastern coasts of Australia and India.

Consistent with the basin averages, the models have different patterns of track density. The GISS model has a similar pattern to the observations, with some key differences. The most striking difference is the lack of a region of high track density off the eastern coast of Central America, which is notoriously difficult to simulate with lower resolution GCMs (Camargo et al. 2005). Other differences include a higher density around India, the region of high density off the eastern coast of Asia extending further to the east, and a lower density in the North Atlantic. The HiRAM model has a remarkably similar pattern to the observations globally. The FSU model has higher density in the North Atlantic and South Indian along with lower density off the eastern coast of Central America. The ECHAM5 model has very low density in the North Atlantic and South Indian, but similar density patterns to the observations in the Western Pacific and South Pacific. The ECHAM5 model also has a localized region of very high density directly on the eastern coast of India. The high resolution CAM5.1 model has a region of very high density off the western coast of Central America that extends too far westward and has much lower density off the eastern coast of Asia than the observations. The low resolution HadGEM3 model has small regions of high density in the correct locations. The higher resolution HadGEM3 models have higher density in these regions, which expand covering larger areas. The global mean density in the lower resolution CAM5.1, GEOS-5, and GFS models are much lower than observed.

In addition to track density, it is useful to study where the simulated TCs form, or genesis density. Figures 4 shows the genesis density of all the models and observations. Genesis density is defined as the total number of TCs that form in a 5° x 5° box per year. The overall differences in the patterns of the genesis density between the models and observations are similar to the differences in the track density described above. Consistent with the observations, all the models have narrower meridional bands of high genesis density as compared to track density. This occurs because the TCs tend to form in low-latitudes and travel poleward, causing the track density to have a greater meridional spread than the genesis density.

It can be easier to distinguish patterns in the distributions by examining certain spatial or temporal dimensions. The top panel of Fig.5 shows the genesis as a function of latitude of each model and the observations. Only the highest resolution simulations of the CAM5.1 and HadGEM3 models are shown. The observations have a large peak at 10° north, a smaller peak at 10° south, and no TC formation directly at the equator. All of the models have peaks at roughly the same latitudes as the observations, with the exception of the FSU model, whose peaks are closer to the equator, and the ECHAM5 model, whose peaks are further poleward than the observations. In addition, the FSU model is the only model that has significant non-zero genesis at the equator. The ECHAM5 model's southern hemisphere peak has a fatter tail and has non-zero genesis extending to higher latitudes than the observations and all other models. Although the GEOS-5 and NCEP models have fewer TCs than in observations, but the maxima in genesis location occur at roughly the same latitudes and with similar relative magnitude as the observations.

The middle panel of Fig.5 shows the genesis as a function of longitude for the models and observations. The observations have two sharp peaks at roughly 90° and 250° (corresponding to the maxima in the South Indian and western coast of Central America in Fig. 4), a broader peak at roughly 150° (corresponding to the maxima off the eastern coast of Asia in figure 4), and near-zero genesis near the dateline. Three of the models (GISS, FSU, and ECHAM5) have much lower Central American 250° peak than the observations, with the GISS model producing virtually no TCs. The FSU model has peaks at 55° (off the eastern coast of Africa) and 310° (North Atlantic) that are not present in any other model or the observations. The ECHAM5 model has a very strong peak at 85° (off the eastern coast of India). The HiRAM model exhibits a pattern remarkably similar to the observations.

Another metric of interest is the seasonal cycle of TC formation. The bottom panel of Fig. 5 shows global genesis as a function of month for models and observations. The observations show a fairly smooth seasonal cycle with a clear maximum between August and September and a minimum around April. In general, the models have a significantly weaker seasonal cycle than the observations, i.e. the difference between the number of TCs in the second half of the year and the first half of the year is less than the difference in the observations.

The TC seasonal cycle varies in the different basins, so we examine the seasonal cycle in each basin individually in Figure 6. The basins in the northern hemisphere typically have a broad peak in the second half of the year and few TCs in the first half of the year, with exception of the North Indian Ocean. In the Western North Pacific, the GISS, HiRAM, FSU, HR HadGEM3, and ECHAM5 models are able to roughly reproduce the peak in the second half of the year, while the other models have no peak. In the Eastern North Pacific, the HiRAM3, HR HadGEM3, HR CAM5.1, and GFS models are able to reproduce the August peak while the other models have very low density throughout the year in this basin. In the North Atlantic, the HiRAM3, FSU, HR CAM5.1, and GFS models reproduce the second half of the year peak. Also of note is that the FSU model has a peak in the Western North Pacific that is roughly three months later than in observations, while it has a peak in the North Atlantic roughly one month earlier than observed. Most models are able to capture the bimodal distribution in the North Indian Ocean, with exception of the ECHAM5. All models are able to reproduce the observed peak in the early part of the year in the South Pacific and Australian basins. In contrast, in the South Indian basin, the CAM5.1 and FSU models have the wrong seasonality with a peak in the second half of the year.

#### 2) TC Intensity

Along with the frequency of TCs, it is important to examine TC intensity. Although the global climate models here are considered "high-resolution", it is not expected that they would be able to reproduce the most intense TCs (category 4 and 5 hurricanes), which would require even higher resolution to be able to simulate those intensities (see e.g. Bender et al. (2010)). A significant fraction of the models here do not come anywhere near those intensities.

The accumulated cyclone energy (ACE) of a TC is the sum of the squares of the TC's maximum wind speed, sampled at 6-hourly intervals whenever the maximum wind speed is at least tropical storm strength (35 kt). Adding the ACE of individual TCs can produce a total ACE for a spatial or temporal region, e.g. a basin ACE or a seasonal ACE. Thus, a larger value of total ACE could correspond to stronger TCs, more TCs, and/or TCs that last longer. Figure 7 shows the total ACE (averaged per year) for each basin. The top panel shows the total ACE of each basin and the bottom panel shows the percentage of the global ACE that occur in each basin. The observations have large values of ACE in the Western North Pacific and South Pacific, a low ACE in the North Indian, and roughly 10% of the global ACE in each of the other four basins. All models are able to reproduce the large ACE percentage in the Western North Pacific, with the ECHAM5 and FSU models having a very low ACE percentage in the Easter North Pacific. Only the ECHAM5 model has a relatively large ACE percentage in the South Pacific, while the GEOS-5 model has an anomalously high ACE percentage in the North Indian Ocean.

The top panel of figure 8 shows the distribution of the maximum wind speed achieved by each TC in all models and the observations. The vertical lines represent boundaries of the Saffir-Simpson hurricane intensity scale (Saffir 1977). The models seems to separate into four regimes of intensities. The HR CAM5.1 has an intensity distribution similar to observations, with a significant number of category 2 hurricanes and even the ability to produce the most intense TCs, i.e. categories 4 and 5 storms. The HiRAM, FSU, and HR HadGEM3 models have many tropical storms and category 1 TCs and some category 2 TCs. The ECHAM5, GEOS-5, and GFS models have mostly tropical storms. The GISS model's TCs are almost all of tropical depression intensity, with only a very small number of weak tropical storms. The difference between the intensity distributions among the models can not simply be a result of the models' resolution. For example, the GEOS-5 model has a horizontal resolution similar to the HiRAM model, but has significantly weaker TCs. On the other hand, the FSU models has some of the strongest TCs, but does not have one of the highest resolutions among the models.

In order to better understand the effect of model resolution on simulated TC intensities, it is instructive to examine the differences in the intensity distributions of the models in multiple horizontal resolutions. Histograms of the maximum wind speeds for the CAM5.1 and HadGEM3 models in various resolutions are shown in the middle and bottom panels of Fig. 8. As expected, both the CAM5.1 and HadGEM3 models show an increase in the mean TC intensity with higher resolution. The increase in intensity of the HR HadGEM3 and HR CAM5.1 models can be also seen as an elongation of the tails of the distributions into higher TC categories.

#### 3) TC life-time

TC life-time distributions in models and observations are shown in Fig. 9, with the TC life-time histograms of the CAM5.1 and HadGEM3 models in different resolution given in the middle and bottom panels, respectively. There is a large variation in the TC life-time among the models. The ECHAM5, GISS, and HR HadGEM3 models have TCs lasting longer than 40 days, while the GEOS-5 and GFS models have very few TCs lasting more than 10 days. This is most likely due to the different tracking schemes used, as they consider different criteria for when to form and end a TC. Of particular note is that for the models with simulations in multiple resolutions, the TCs in the higher resolution simulations have a slightly longer average duration than in the low-resolution ones.

### *b. Interannual variability*

In the previous section, we analyzed the model simulations forced with climatologically SSTs, which characterizes the typical TC properties in the models, but does not simulate the TC interannual variability. Well known modes of climate variability in the atmosphere and ocean, most notably the El-Niño Southern Oscillation (ENSO), have been shown to affect the frequency and characteristics of TCs (Camargo et al. 2010). In order to evaluate the ability of the models to accurately simulate the interannual variability of TCs, the models were also run while forced with historical monthly varying SST, as opposed to climatological mean SSTs. The number of ensemble members and years of the simulations are shown in Table 2.

Figure 10 shows the total number of TCs globally per year for the models and observations (top panel), as well as for the Western North Pacific, Eastern North Pacific, and North Atlantic, separately[1,2]. The global number of TCs in the models is similar to the observed numbers in all the models, but the global interannual variability is not well captured by the models. The three individual basins shown here present a greater similarity between the observations and model results, with the exception of the GISS model which has very few TCs in the North Atlantic and Eastern North Pacific and the FSU model which has very few TCs in the Eastern North Pacific.

In order to quantify the ability of the models to reproduce the interannual variability of observed TCs in different basins, we calculate the correlation coefficient between the models and observations ACE per year in each basin in Table 3. Since the GISS model's TCs have very weak intensities that seldom exceed the ACE threshold of 35 kt, we define another metric, the model-ACE (MACE), as the sum of the squares of the TC's maximum wind speed, sampled at 6-hourly intervals without any intensity threshold (as was done in **?** for low-resolution models). The correlations of the models' yearly MACE in each basin with the yearly ACE of the observations also shown in Table 3. The correlations in the North Atlantic and Pacific basins are much higher than the other basins. In particular, the FSU and HiRAM models have a correlation coefficient of 0.7 in the North Atlantic and the GEOS-5 model has a correlation coefficient of 0.7 in the Western North Pacific basin.

Figure 11 shows the difference of genesis density for El Niño and La Niña years. El Niño and La Niña seasons are defined for the northern and southern Hemispheres in table 4[3]. The

[1]The FSU model interannual simulation was only performed between June and November of each year and the tracking scheme was only done in the North Atlantic and North Pacific basins.

[2]The GEOS-5 model used different physical parametrizations (minimum entrainment threshold for parameterized deep convection in the modified Relaxed Arakawa-Schubert convection scheme, as well as a different time step) in the climatological and interannual simulations, which led a very different TC global frequency between those runs.

[3]Using the warm and cold ENSO (El Niño Southern Oscillations) definitions of the Climate Prediction Center, available at `http://www.cpc.ncep.noaa.gov/products/analysis_monitoring/ensostuff/ensoyears.shtml`.

observations have a larger and stronger peak in genesis density off of the western coast of Central America in El Niño months than La Niña months. As the GISS and FSU models have very few TCs in this region, they are unable to reproduce this difference, while the HiRAM and GEOS-5 models are able to reproduce the difference.

A well known impact of ENSO on TC development is for average formation location to shift to the south and east in the Western North Pacific and to shift to the south and west in the Eastern North Pacific during El Niño years (Chia and Ropelewski 2002). Figure 12 shows the mean position of TC formation in the Western and Eastern North pacific, split between La Niña and El Ñino years. In the Western North Pacific, the models are able to reproduce the southwest shift in El Niño years, with exception of the FSU model which has an eastern shift. In the Eastern North Pacific, all the models are able to simulate the southwest shift in El Niño years.

# 4. Conclusions

This work has described an intercomparison of several high-resolution atmospheric models of the present climate, forced with both climatological and historical SSTs, in their ability to simulate the characteristics of TCs seen in observations. Model TCs were compared to observational TCs in terms of frequency as well as spatial, temporal, and intensity distributions. A range of tracking schemes were applied by each individual group to derive TC tracks and intensities for all models, consistent with the way in which results from these models have been shown previously in single-model studies.

Overall the models were able to reproduce the geographic distribution of TC track density in the observations, with the HiRAM model, in particular, demonstrating the most similarity to observations. TC formation off the eastern coast of Central America was the most difficult region to correctly simulate, with the HiRAM, HR CAM5.1, and HadGEM3 models demonstrating superior performance.

All models have a weaker seasonal cycle than observations, with relatively too few TCs in the second half of the year and relatively too many TCs in the first half of the year. The models reproduce the observational seasonal cycle to varying degrees in each basin, with the HiRAM model showing arguably the best match to observations overall.

There is a wide range in TC intensities between the different models. Some, but not all, of this difference can be seen as a consequence of resolution, with higher resolution models being able to simulate stronger TCs. This effect can be most readily seen in the CAM5.1 and HadGEM3 models which were run at multiple resolutions.

In the simulations forced with historical SSTs, the models were able to reproduce the interannual variability of TC frequency in the North Pacific and Atlantic basins, with the HiRAM and GEOS-5 models showing particularly high correlation with observations in those basins. All models were also able to reproduce the general geographic shift in TC formation location during El Niño and La Niña years.

*Acknowledgments.*

The authors would like to thank all members of the U.S. CLIVAR Hurricane Working Group for their contribution to this significant effort. We also would like to thank Naomi Henderson for making the model data available for the working group and managing the dataset. DAS, SJC and AHS acknowledge support of NSF AGS 1143959.

# REFERENCES

Bender, M. A., T. R. Knutson, R. E. Tuleya, J. J. Sirutis, G. A. Vecchi, S. T. Garner, and I. M. Held, 2010: Modeled impact of anthropogenic warming on the frequency of intense Atlantic hurricanes. *Science*, **327**, 454.

Bengtsson, L., H. Böttger, and M. Kanamitsu, 1982: Simulation of hurricane-type vortices in a general circulation model. *Tellus*, **34**, 440–457.

Bengtsson, L., K. I. Hodges, and M. Esch, 2007a: Tropical cyclones in a T159 resolution global climate model: Comparison with observations and re-analysis. *Tellus*, **59 A**, 396 – 416.

Bengtsson, L., K. I. Hodges, M. Esch, N. Keenlyside, L. Kornblueh, J.-J. Luo, and T. Yamagata, 2007b: How many tropical cyclones change in a warmer climate? *Tellus*, **59 A**, 539 – 561.

Camargo, S. J., 2013: Global and regional aspects of tropical cyclone activity in the CMIP5 models. *J. Climate*, **26**, 9880–9902.

Camargo, S. J. and A. G. Barnston, 2009: Experimental seasonal dynamical forecasts of tropical cyclone activity at IRI. *Wea. Forecasting*, **24**, 472 – 491.

Camargo, S. J., A. G. Barnston, and S. E. Zebiak, 2005: A statistical assessment of tropical cyclones in atmospheric general circulation models. *Tellus*, **57A**, 589–604.

Camargo, S. J., A. H. Sobel, A. G. Barnston, and P. J. Klotzbach, 2010: The influence of natural climate variability on tropical cyclones and seasonal forecasts of tropical cyclone activity. *Global Perspectives on Tropical Cyclones, from Science to Mitigation*, J. C. L.

Chan and J. D. Kepert, Eds., World Scientific, Series on Earth System Science in Asia, 2d ed., chap. 11, 325–360.

Camargo, S. J. and S. E. Zebiak, 2002: Improving the detection and tracking of tropical storms in atmospheric general circulation models. *Wea. Forecasting*, **17**, 1152–1162.

Chia, H. H. and C. F. Ropelewski, 2002: The interannual variability in the genesis location of tropical cyclones in the Northwest Pacific. *J. Climate*, **15**, 2934–2944.

Chu, J.-H., C. R. Sampson, A. S. Levine, and E. Fukada, 2002: The Joint Typhoon Warning Center tropical cyclone best-tracks, 1945-2000. Tech. Rep. NRL/MR/7540-02-16, Naval Research Laboratory.

Emanuel, K., 2003: Tropical cyclones. *Ann. Rev. Earth Planet. Sci.*, **31**, 75–104.

Hodges, K. I., 1995: Feature tracking on the unite sphere. *Mon. Wea. Rev.*, **19**, 5686–5699.

JTWC, 2013: Joint Typhoon Warning Center Tropical Cyclone Best Track Data Site. Joint Typhoon Warning Center, Available online at http://www.npmoc.navy.mil.

Landsea, C. W. and J. L. Franklin, 2013: Atlantic hurricane database uncertainty and presentation of a new database format. *Mon. Wea. Rev.*, **141**, 3576–3592.

LaRow, T. E., Y.-K. Lim, D. W. Shin, E. P. Chassignet, and S. Cocke, 2008: Atlantic basin seasonal hurricane simulations. *J. Climate*, **21**, 3191–3206.

Manabe, S., J. L. Holloway, and H. M. Stone, 1970: Tropical circulation in a time-integration of a global model of the atmosphere. *J. Atmos. Sci.*, **27**, 580–613.

Mizuta, R., et al., 2012: Climate simulations using the improved MRI-AGCM with 20-km grid. *J. Meteor. Soc. Japan*, **90A**, 235–260.

Murakami, H., et al., 2012: Future changes in tropical cyclone activity projected by the new high-resolution MRI-AGCM. *J. Climate*, **25**, 3237–3260.

NHC, 2013: NHC (National Hurricane Center) best track dataset. National Hurricane Center, available online at http://www.nhc.noaa.gov.

Prabhat, O. Rubel, S. Byna, K. S. Wu, M. Wehner, and W. Bethel, 2012: TECA: A Parallel Toolkit for Extreme Climate Analysis. *Proc. Int. Conf. on Computational Science, ICCS 2012*, H. Ali, Y. Shi, D. Khazanchi, M. Lees, G. VanAlbada, J. Dongarra, and P. M. A. Sloot, Eds., Procedia Computer Science, Vol. 9, 866–876, doi:{10.1016/j.procs.2012.04.093}.

Rayner, N. A., D. E. Parker, E. B. Horton, C. K. Folland, L. V. Alexander, D. P. Rowell, E. C. Kent, and A. Kaplan, 2003: Global analyses of sea surface temperature, sea ice, and night marine air temperature since the late nineteenth century. *Journal of Geophysical Research: Atmospheres*, **108 (D14)**, 2156–2202.

Rienecker, M., et al., 2008: The GEOS-5 Data Assimilation System - Documentation of Versions 5.0.1, 5.1.0, and 5.2.0. *Technical Report Series on Global Modeling and Data Assimilation*, **27**.

Roeckner, E. e. a., 2003: The atmospheric general cir- culation model ECHAM5. Part I: Model description. *MPI*, **349**, 127 pp.

Saffir, H. S., 1977: Design and construction requirements for hurricane resistant construction. Tech. Rep. Preprint No. 2830, 20 pp., ASCE. Available from American Society of Civil Engineers, New York, NY 10017.

Saha, S., et al., 2013: The ncep climate forecast system version 2. *J. Climate*, **revised**.

Schmidt, e. a., G.A., 2013: Configuration and assessment of GISS ModelE2 contributions to the CMIP5 archive. *J. Climate*, submitted.

Scoccimarro, E., et al., 2011: Effects of tropical cyclones on ocean heat transport in a high resolution coupled general circulation model. *J. Clim.*, **24**, 4368–4384.

Strachan, J., P. L. Vidale, K. Hodges, M. Roberts, and M.-E. Demory, 2013: Investigating global tropical cyclone activity with a hierarchy of AGCMs: the role of model resolution. *J. Climate*, **26**, 133–152.

Vitart, F., D. Anderson, and T. Stockdale, 2003: Seasonal forecasting of tropical cyclone landfall over Mozambique. *J. Climate*, **16**, 3932–3945.

Vitart, F., J. L. Anderson, and W. F. Stern, 1997: Simulation of interannual variability of tropical storm frequency in an ensemble of GCM integrations. *J. Climate*, **10**, 745–760.

Vitart, F., et al., 2007: Dynamically-based seasonal forecasts of Atlantic tropical storm activity issued in june by EUROSIP. *Geophys. Res. Lett.*, **34**, L16 815.

Walsh, K., 1997: Objective detection of tropical cyclones in high-resolution analyses. *Mon. Wea. Rev.*, **125**, 1767–1779.

Walters, D., et al., 2011: The Met Office Unified Model Global Atmosphere 3.0/3.1 and JULES Global Land 3.0/3.1 configurations. *Geosci. Model Dev.*, **4**, 919–941.

Wehner, M. F., et al., 2013: The effect of horizontal resolution on simulation quality in the Community Atmospheric Model, CAM5.1. *Journal of Modeling the Earth System*, to be submitted.

Zhao, M., I. M. Held, S.-J. Lin, and G. A. Vecchi, 2009: Simulations of global hurricane climatology, interannual variability and response to global warming using a 50 km resolution gcm. *J. Climate*, **22**, 6653–6678.

TABLE 1. Table of model parameters. LR: Low Resolution, MR: Medium Resolution, HR: High Resolution. Roeckner/Scoccimarro: Roeckner (2003) and Scoccimarro et al. (2011). Hodges/Bengtsson: Hodges (1995) and Bengtsson et al. (2007b) . Mizuta/Murakami: Mizuta et al. (2012) and Murakami et al. (2012)

| Model | Resolution | Approx Res (km) | Reference | Tracking Scheme |
|---|---|---|---|---|
| LR CAM5.1 | 100 km | 100 | Wehner et al. (2013) | Prabhat et al. (2012) |
| HR CAM5.1 | 1/4° | 28 | Wehner et al. (2013) | Prabhat et al. (2012) |
| ECHAM5 | T159 | 84 | Roeckner/Scoccimarro | Walsh (1997) |
| FSU | T126 | 106 | LaRow et al. (2008) | Vitart et al. (2003) |
| GEOS-5 | 1/2° | 56 | Rienecker et al. (2008) | Vitart et al. (2003) |
| GFS | T126 | 106 | Saha et al. (2013) | Zhao et al. (2009) |
| GISS | 1° | 111 | Schmidt (2013) | Camargo and Zebiak (2002) |
| LR HadGEM3 | N96 | 130 | Walters et al. (2011) | Hodges/Bengtsson |
| MR HadGEM3 | N216 | 60 | Walters et al. (2011) | Hodges/Bengtsson |
| HR HadGEM3 | N320 | 40 | Walters et al. (2011) | Hodges/Bengtsson |
| HiRAM | 50 km | 50 | Zhao et al. (2009) | Zhao et al. (2009) |
| MRI | TL319 | 60 | Mizuta/Murakami | Murakami et al. (2012) |

# List of Tables

Table 2. Models that performed interannual simulations.

| Model | Number of Ensembles | Years |
|---|---|---|
| FSU | 3 | 1982-2009 |
| GEOS-5 | 2 | 1982-2009 |
| GISS | 3 | 1981-2009 |
| HiRAM | 3 | 1981-2009 |
| MRI | 1 | 1981-2003 |

Table 3. Correlation of yearly ACE and model-ACE (MACE) in each basin and the yearly observed ACE, shown as ACE / MACE. Basins are defined as: SI (South Indian), AUS (Australian), SP (South Pacific), NI (North Indian), WNP (Western North Pacific), ENP (Easter North Pacific), NATL (North Atlantic).

| Model | SI | AUS | SP | NI | WNP | ENP | NATL |
|---|---|---|---|---|---|---|---|
| FSU | - | - | - | - | 0/0 | 0.5*/0.5* | 0.7*/0.7* |
| GEOS-5 | 0/0 | -0.1/-0.2 | 0.5*/0.4* | -0.2/-0.2 | 0.7*/0.7* | 0.4*/0.5* | 0.6*/0.6* |
| GISS | 0/0 | -0.3/0 | -0.2/-0.2 | -0.2/0.2 | 0.3/0.2 | 0/0.7* | 0/0.4 |
| HiRAM | 0.2/0.2 | 0.4*/0.4* | 0.1/0.1 | -0.1/-0.1 | 0.5*/0.5* | 0.6*/0.6* | 0.7*/0.7* |
| MRI | 0.2/0.2 | -0.4*/-0.4* | 0.1/0.1 | -0.1/-0.1 | 0.3/0.3 | 0.4*/0.4* | 0.6*/0.6* |

TABLE 4. El Niño and La Niña seasons for the northern and southern hemispheres, using the warm and cold ENSO (El Niño Southern Oscillations) definitions of Climate Prediction Center. The northern (southern) hemisphere seasons definitions as based on the state of ENSO in the August - October (January - March) seasons. Note that the southern hemisphere TC seasons are defined from July to June, emcompassing 2 calendar years.

| | Northern Hemisphere |
|---|---|
| El Niño | 1982, 1986, 1987, 1991, 1994, 1997, 2002, 2004, 2006, 2009 |
| La Niña | 1983, 1985, 1988, 1995, 1998, 1999, 2000, 2007 |

| | Southern Hemisphere |
|---|---|
| El Niño | 1982/83, 1986/87, 1987/88, 1991/92, 1994/95, 1997/98, 2002/03 |
| La Niña | 1980/81, 1984/85, 1988/89, 1995/96, 1998/99, 1999/00, 2000/01, 2005/06, 2007/08, 2008/09 |

# List of Figures

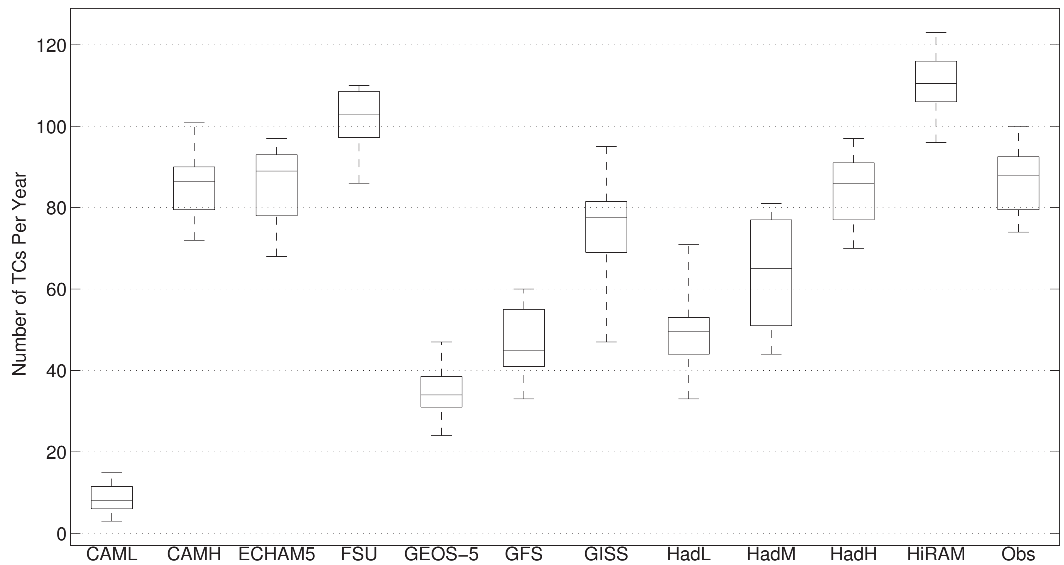


FIG. 1. Distributions of the number of TCs per year for models and observations. The horizontal line inside the boxes shows the median number of TCs per year, the top and bottom of the boxes represent the 75th and 25th percentiles respectively, with the whiskers extending to the maximum and minimum number of TCs per year in each case. CAML: Low-resolution CAM5.1, CAMH: High-resolution CAM5.1, HadL: Low-resolution HadGEM3, HadM: Medium-resolution HadGEM3, HadH: High-resolution HadGEM3.

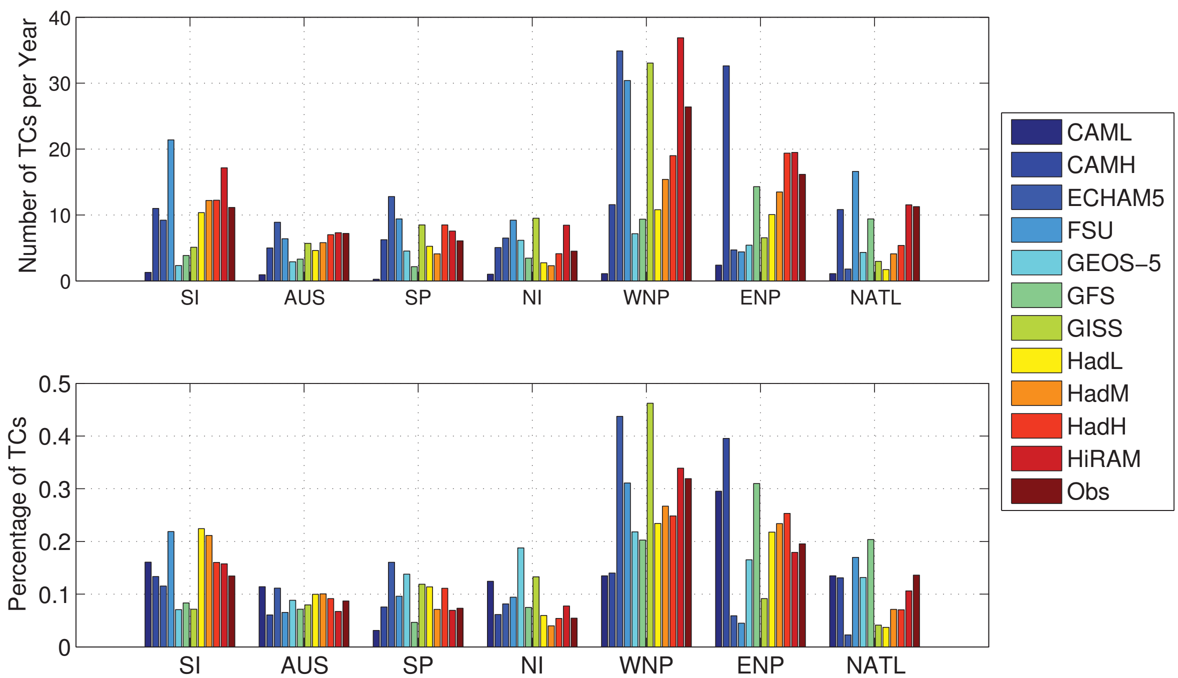


FIG. 2. Mean number of TCs formed in each basin for models and observations. The top panel shows the total number of TCs, while the bottom panel shows the percentage of TCs in each basin. The basins are defined as: SI (South Indian), AUS (Australian), SP (South Pacific), NI (North Indian), WNP (Western North Pacific), ENP (Easter North Pacific), NATL (North Atlantic). The model names follow the definitions in Fig. 1.

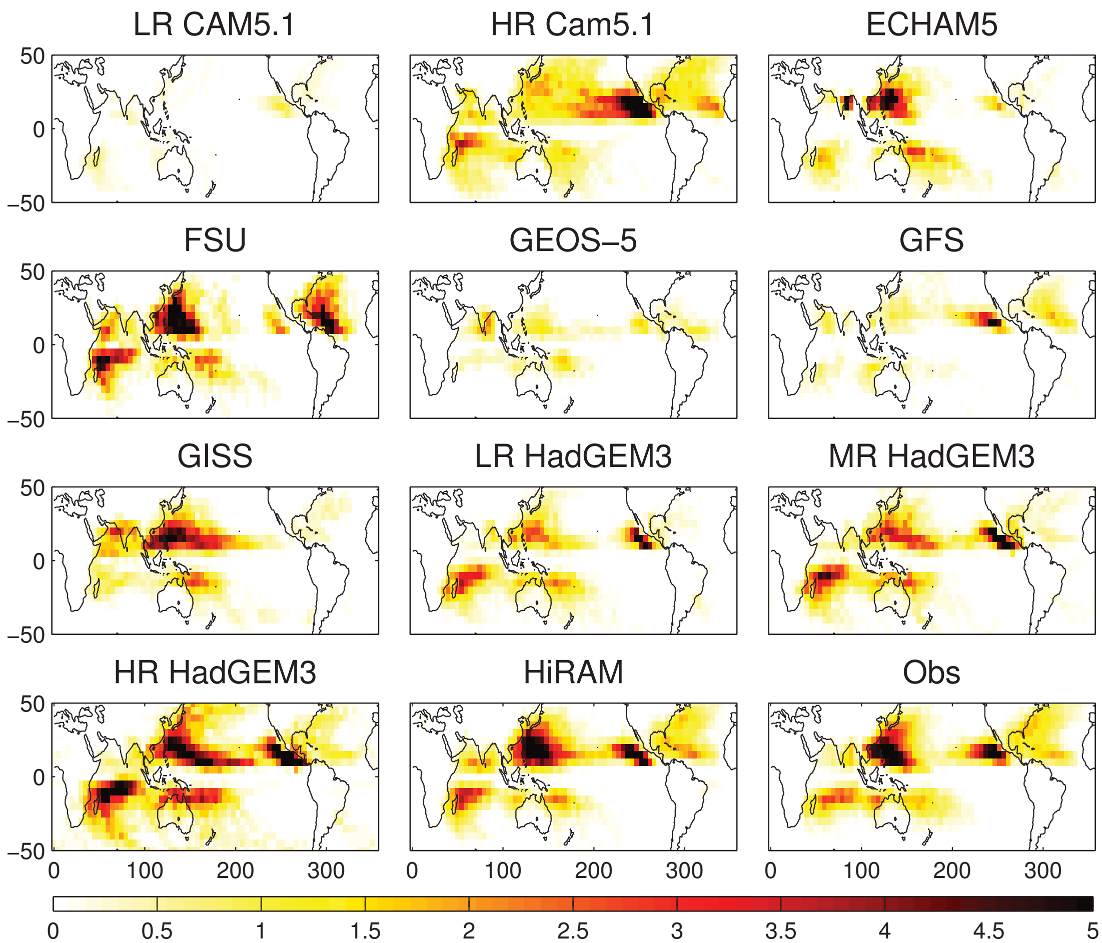


Fig. 3. TC track density in models and observations. Track density is defined as the mean number of TC transits per 5° x 5° box per year.

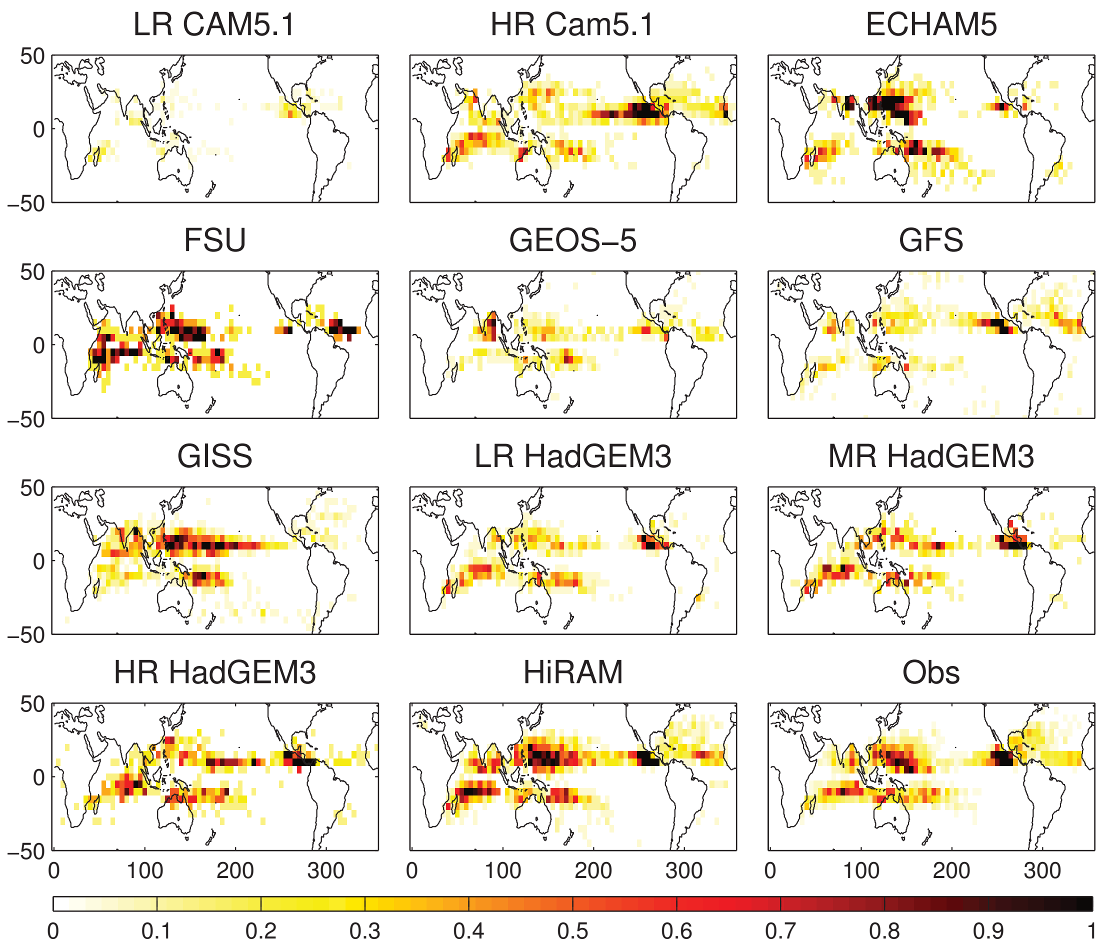


Fig. 4. TC genesis density in models and observations. Genesis density is defined as mean TC formation per 5° x 5° box per year.

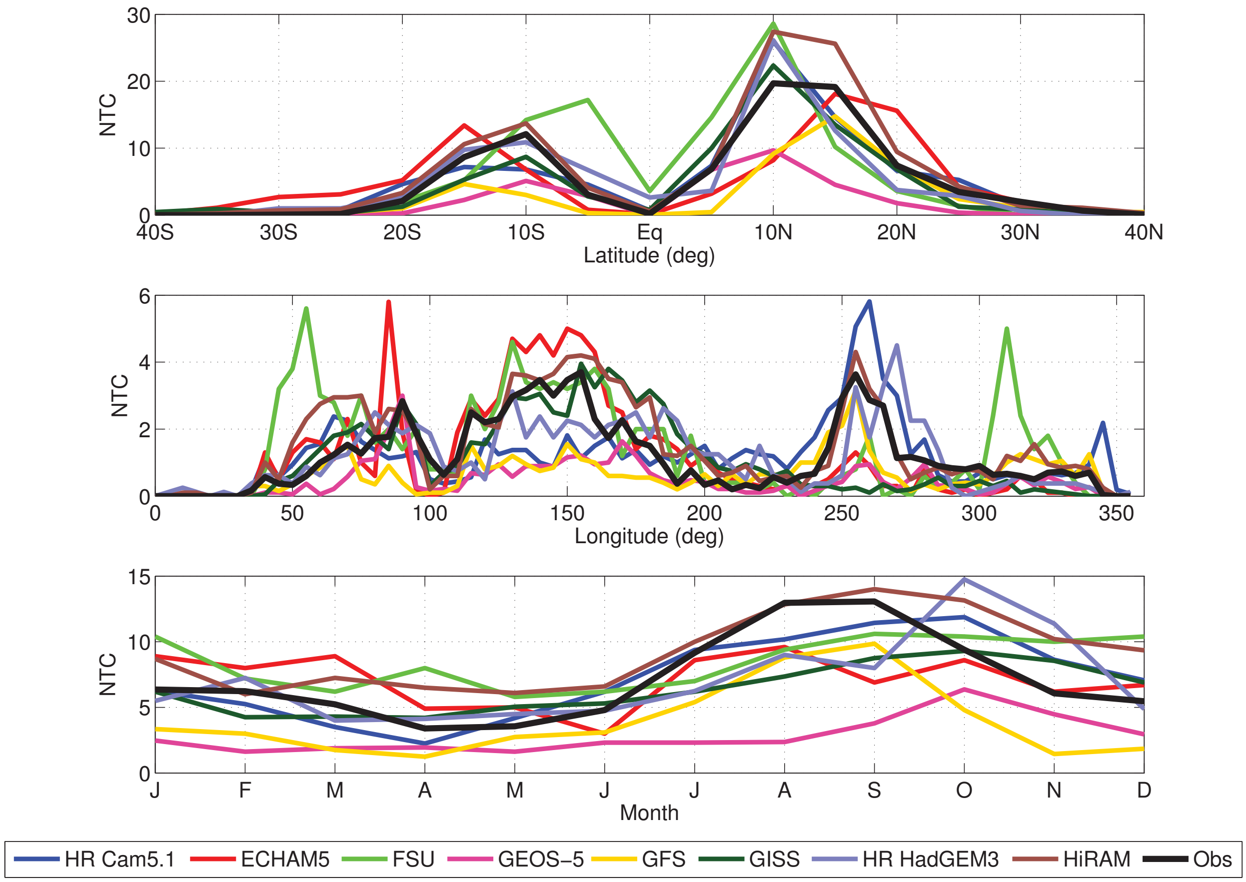


Fig. 5. Mean number of TC genesis per year in models and observations as a function of latitude (top panel), longitude (middle panel), and month (bottom panel).

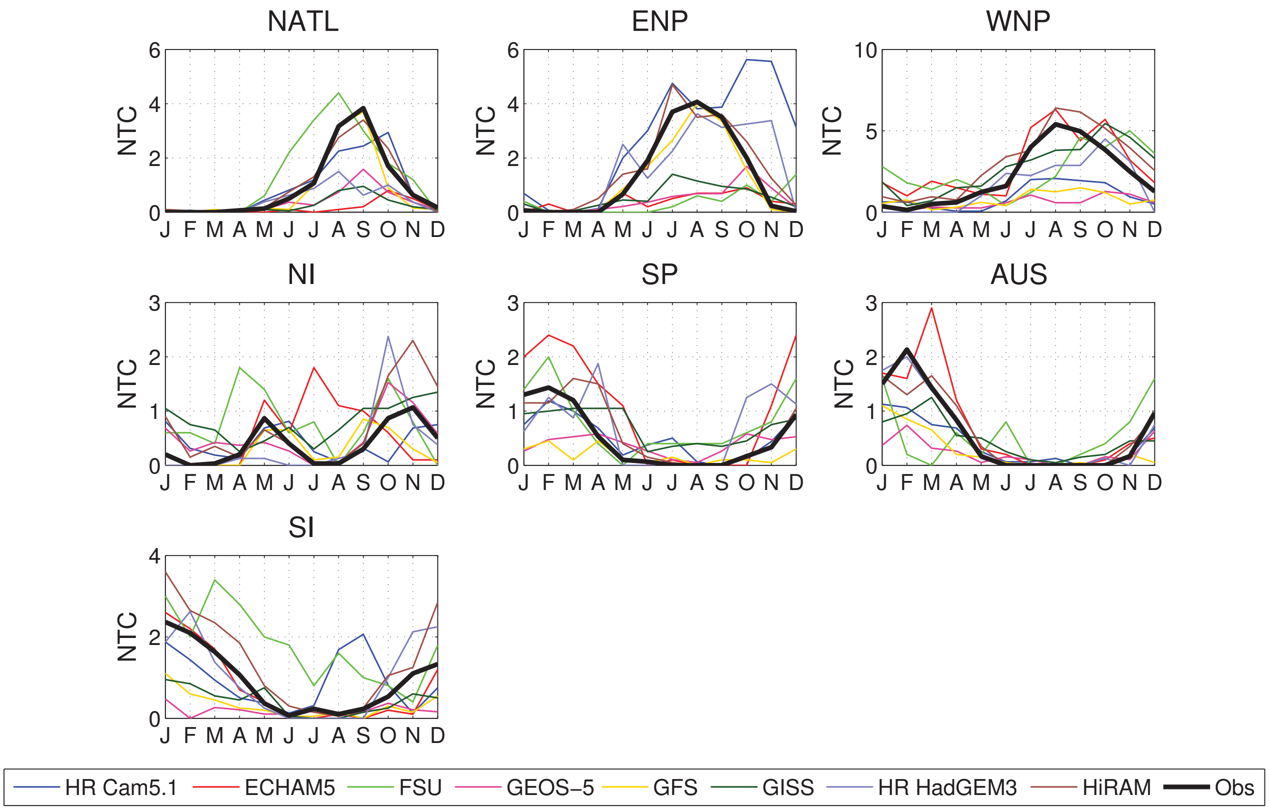


FIG. 6. Mean TC genesis per year and month in models and observation in various basins (as defined in Fig. 1)

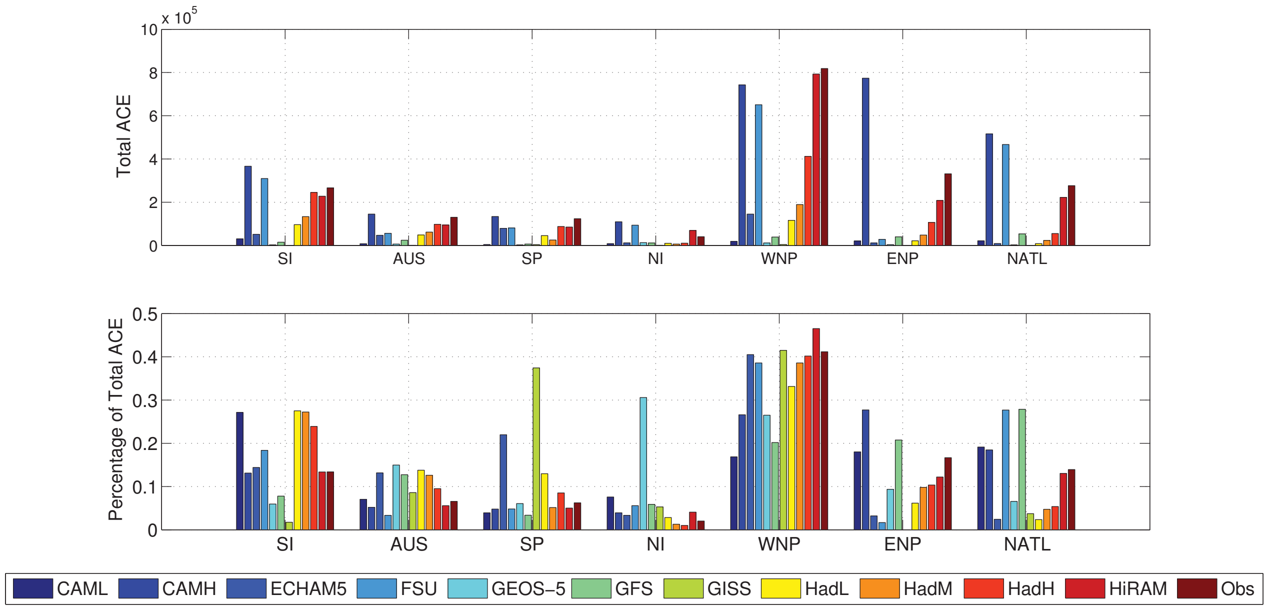


FIG. 7. Total accumulated cyclone energy (ACE) for models and observations (top panel). The bottom panel shows the percentage of the total ACE in each basin for models and observations. Basins and models are defined as in previous Figs.

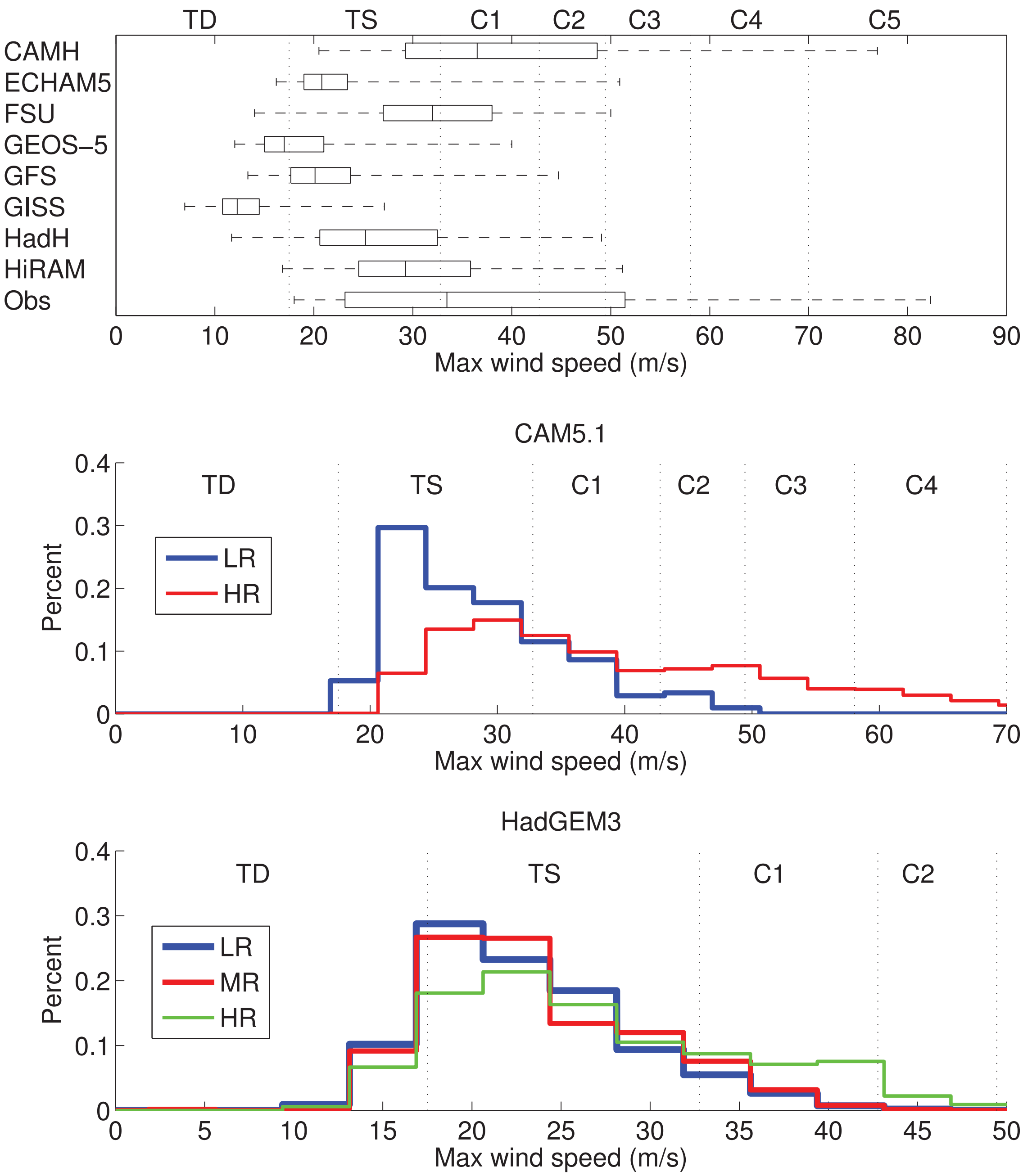


Fig. 8. Distributions of TC maximum intensity in models and observations (top panel). The horizontal line shows the median of each distribution, the left and right edges of the box represent the 75th and 25th percentiles respectively, and the whiskers extend to the maximum and minimum values in each case. Histograms of TC maximum intensity for two horizontal resolutions of the CAM5.1 model (middle panel) and three model resolutions of the HadGEM1 model (bottom panel). The vertical lines show the boundaries of the Saffir-Simpson hurricane classification scale. TD: Tropical Depression, TS: Tropical Storm, C1-C5: Category 1-5 hurricanes. LR: Low resolution, MR: Medium resolution, HR: High resolution.

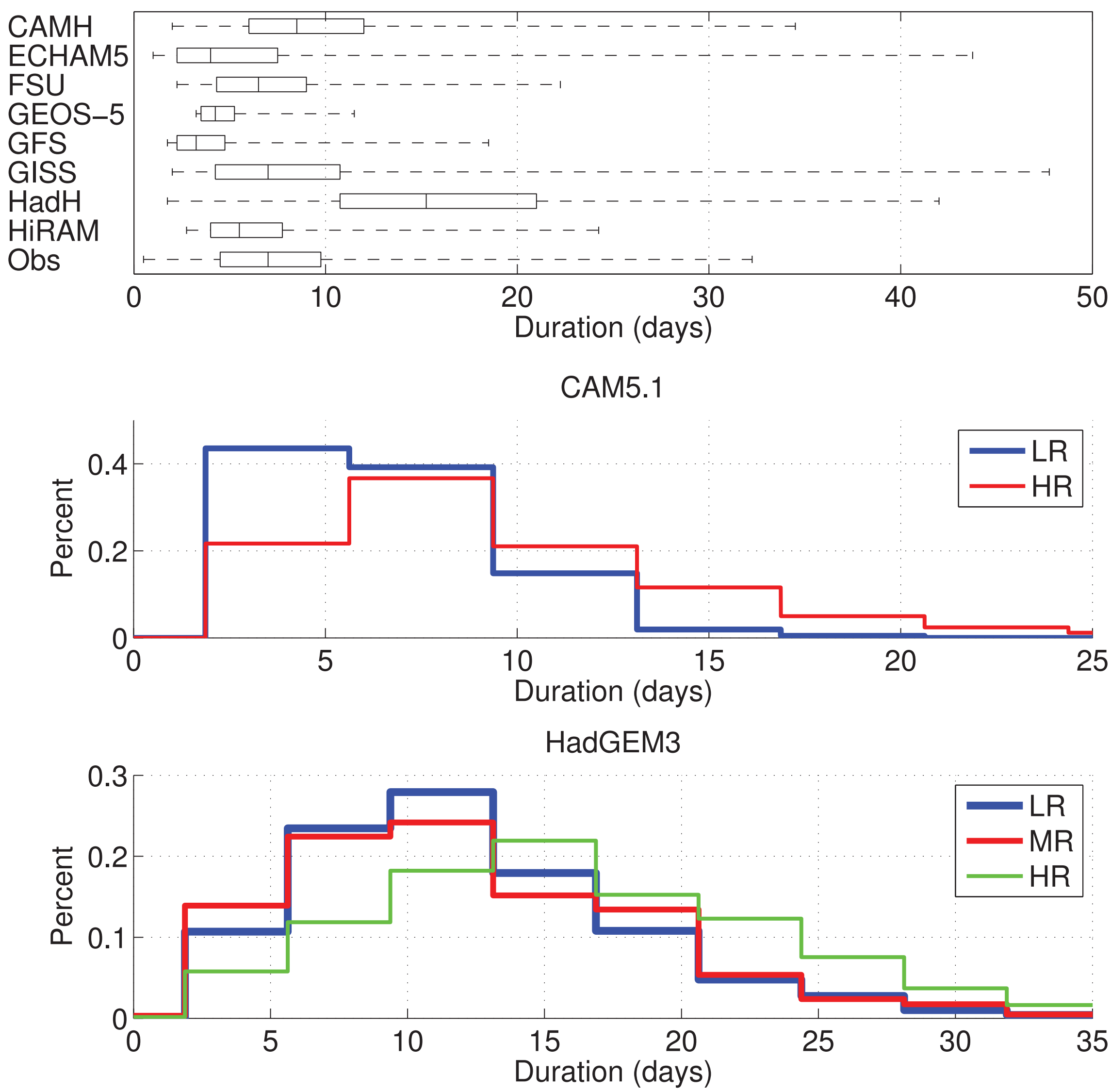


FIG. 9. Distributions of TC life-time (or duration) for models and observations. The horizontal line shows the median of each distribution, the left and right edges of the box represent the 75th and 25th percentiles respectively, and the whiskers extend to the maximum and minimum values in each case. The histograms of TC durations in the CAM5.1 and HadGEM3 models for different resolutions are shown in the middle and bottom panel, respectively. LR: Low resolution, MR: Medium resolution, HR: High resolution.

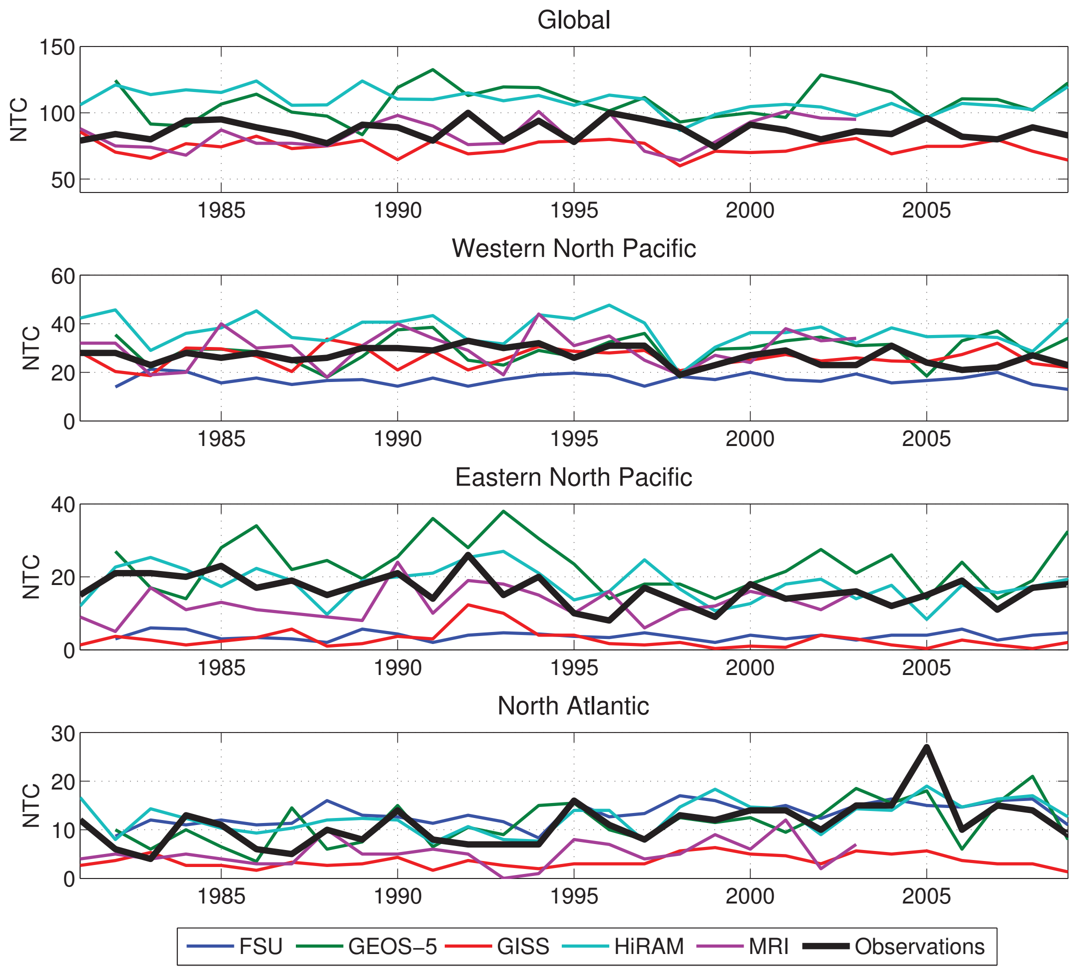


FIG. 10. Number of TCs per year (top panel) in the globe and in a few of the Northern Hemipshere basins (Western North Pacific, Eastern North Pacific, and North Atlantic). For the models, when more than one ensemble simulation was available, the ensemble mean number of TCs in each year is shown.

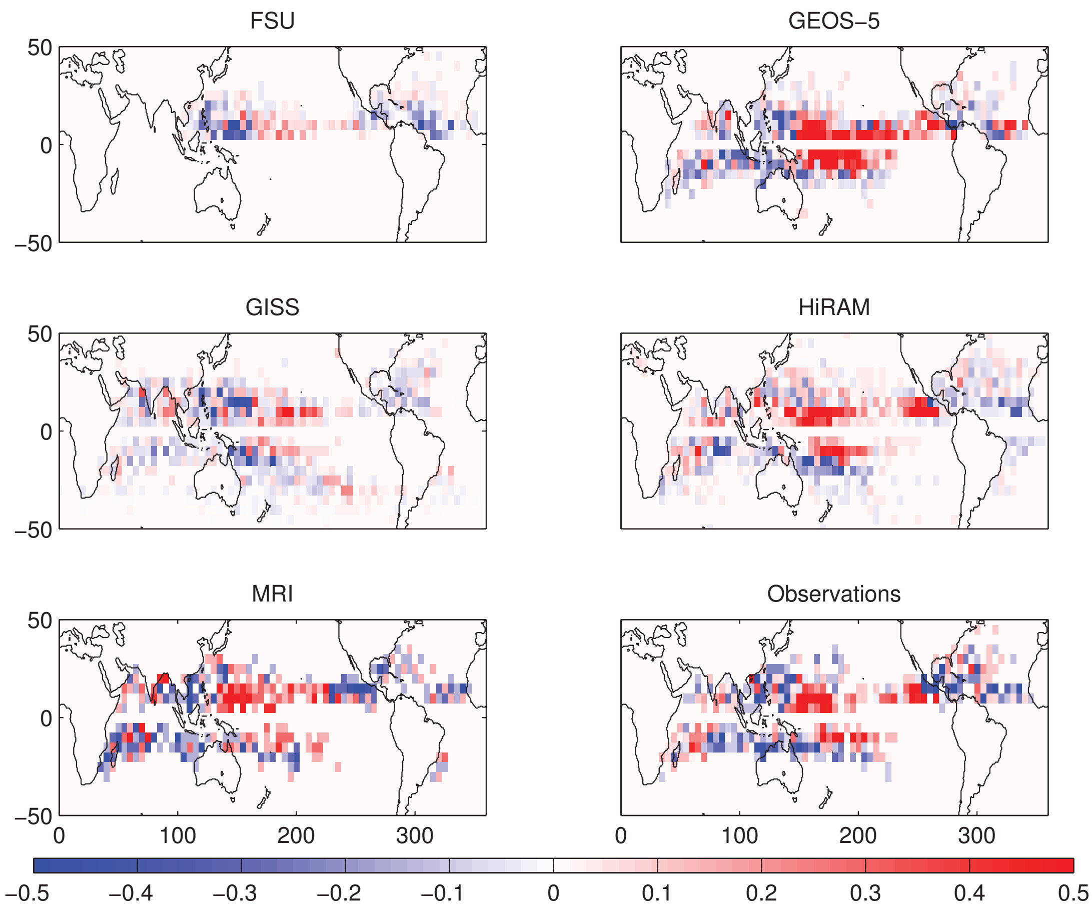


FIG. 11. Difference of TC genesis density in El Niño and La Niña seasons in models and observations. The genesis density is defined as the mean TC formation per 5° x 5° box per year.

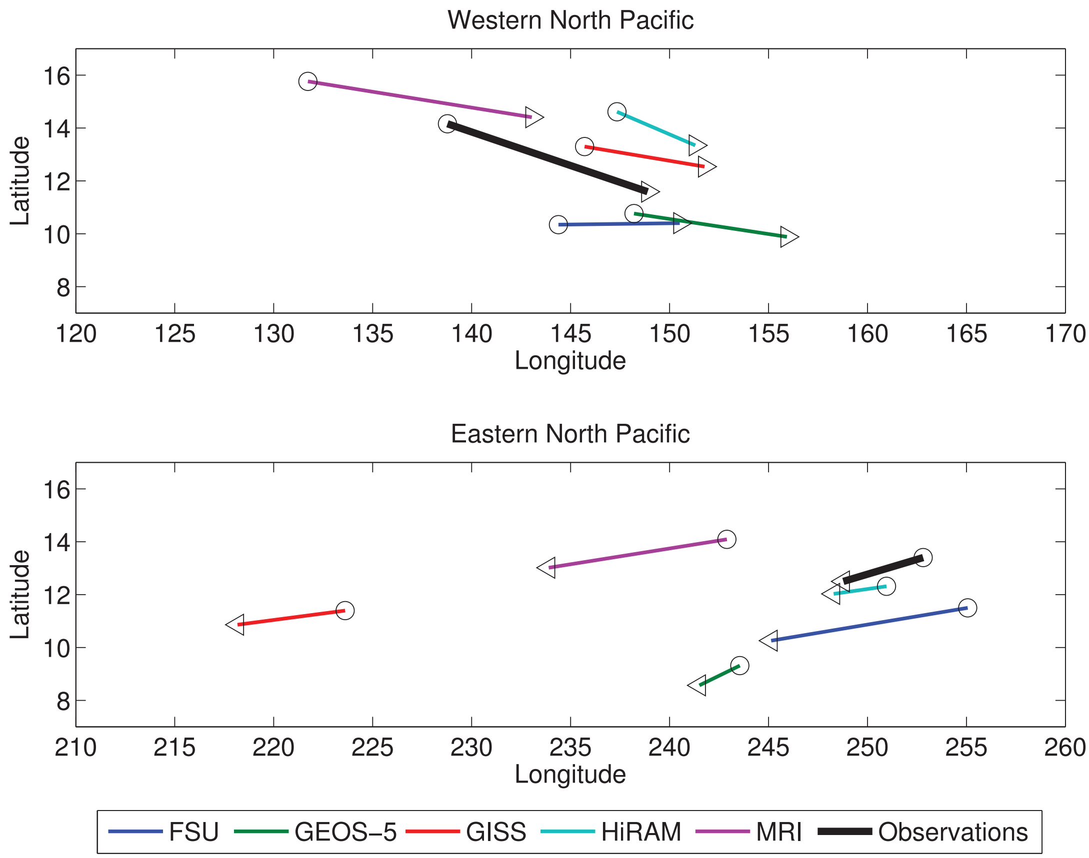


FIG. 12. Mean TC genesis location in the western and eastern North Pacific in El Niño (triangles) and La Niña (circles) years in models and observations.